HHS Public Access

Author manuscript

Sci Transl Med. Author manuscript; available in PMC 2020 January 23.

Published in final edited form as:

Sci Transl Med. 2019 January 23; 11(476): . doi:10.1126/scitranslmed.aav4754.

Cyclin G1 and TASCC regulate kidney epithelial cell G_2-M arrest and fibrotic maladaptive repair

Guillaume Canaud[1,2,3,*], **Craig R. Brooks**[1,4,*], **Seiji Kishi**[1,5,*], **Kensei Taguchi**[4], **Kenji Nishimura**[5], **Sato Magassa**[2], **Adam Scott**[1,6], **Li-Li Hsiao**[1], **Takaharu Ichimura**[1], **Fabiola Terzi**[2], **Li Yang**[7], and **Joseph V. Bonventre**[1,8,9,†]

[1]Renal Division, Brigham and Women's Hospital, Department of Medicine, Harvard Medical School, Boston, MA 02115, USA

[2]INSERM U1151, Institut Necker-Enfants Malades, Université Paris Descartes, Paris 75743, France

[3]Service de Néphrologie et Transplantation Adultes, Hôpital Necker-Enfants Malades, Paris 75743, France

[4]Division of Nephrology and Hypertension, Department of Medicine, Vanderbilt University Medical Center, Nashville, TN 37232, USA

[5]Department of Nephrology, Graduate School of Biomedical Sciences, Tokushima University, Tokushima 7708503, Japan

[6]Division of Nephrology, Department of Medicine, Boston Children's Hospital, Harvard Medical School, Boston, MA 02115, USA

[7]Renal Division, Peking University First Hospital, Beijing 100871, China

[8]Division of Health Sciences and Technology, Harvard-Massachusetts Institute of Technology, Cambridge, MA 02139, USA

[9]Harvard Stem Cell Institute, Cambridge, MA 02138, USA

Abstract

Fibrosis contributes to the progression of chronic kidney disease (CKD). Severe acute kidney injury can lead to CKD through proximal tubular cell (PTC) cycle arrest in the G_2-M phase, with secretion of profibrotic factors. Here, we show that epithelial cells in the G_2-M phase form target

† Corresponding author. joseph_bonventre@hms.harvard.edu.

*These authors contributed equally to this work as co-first authors.

Author contributions: G.C., C.R.B., S.K., and J.V.B. conceptualized and designed the study. G.C., C.R.B., S.K., K.T., K.N., and S.M. conducted the experiments. L.-L.H. performed the DNA microarrays. G.C., C.R.B., S.K., K.T., K.N., S.M., A.S., T.I., F.T., L.Y., and J.V.B. analyzed the data. G.C., C.R.B., S.K., and J.V.B. wrote the manuscript. All authors helped to interpret results and approved the final version of the manuscript.

Data and materials availability: All data associated with this study are present in the paper or Supplementary Materials. Microarray data are available from GEO (series accession number: GSE5350). Original materials created in this study will be made available to the scientific community in accordance with the institution's guidelines. Materials used in this study that were created by other researchers will be made available in accordance with the originating organization's agreements and subject to their terms and conditions.

SUPPLEMENTARY MATERIALS

www.sciencetranslationalmedicine.org/cgi/content/full/1¼76/eaav4754/DC1

of rapamycin (TOR)–autophagy spatial coupling compartments (TASCCs), which promote profibrotic secretion similar to the senescence-associated secretory phenotype. Cyclin G1 (CG1), an atypical cyclin, promoted G_2-M arrest in PTCs and up-regulated TASCC formation. PTC TASCC formation was also present in humans with CKD. Prevention of TASCC formation in cultured PTCs blocked secretion of profibrotic factors. PTC-specific knockout of a key TASCC component reduced the rate of kidney fibrosis progression in mice with CKD. CG1 induction and TASCC formation also occur in liver fibrosis. Deletion of CG1 reduced G_2-M phase cells and TASCC formation in vivo. This study provides mechanistic evidence supporting how profibrotic G_2-M arrest is induced in kidney injury and how G_2-M–arrested PTCs promote fibrosis, identifying new therapeutic targets to mitigate kidney fibrosis.

One-sentence summary

Cyclin G1 regulates G_2-M arrest in proximal tubular cells, promoting a TASCC-induced secretory phenotype, fibrosis, and kidney disease progression.

Editor's Summary

Taking kidney fibrosis to TASCC

The kidney has an inherent capacity to recover from acute injury; however, severe injury can lead to chronic kidney disease and fibrosis. Canaud *et al.* studied kidney epithelial cells' maladaptive response to injury. The formation of target of rapamycin-autophagy spatial coupling compartments (TASCCs) in proximal epithelial cells was associated with cell cycle arrest and fibrosis in human chronic kidney disease, whereas knocking out cyclin G1 prevented TASCC formation and fibrosis in mouse models. This study provides mechanistic insight into renal fibrosis and identifies a potential therapeutic target.

INTRODUCTION

Acute kidney injury (AKI) had long been thought to be a completely reversible process, whereby resident kidney cells could repair the kidney after an ischemic or a toxic insult to fully restore renal function. During the last two decades, however, animal and human studies have linked AKI to chronic kidney disease (CKD) *(1–4).* CKD represents a worldwide health concern affecting more than 20 million Americans and about 10% of the global population, resulting in a rapidly increasing burden of associated cardiovascular diseases, end-stage kidney disease, mortality, and growing societal financial burden (*5, 6*). Understanding the pathophysiology of CKD is of great importance to ultimately prevent and arrest its progression.

Injury causes tubular cells, especially proximal tubular cells (PTCs), to lose their polarity and brush border (7), alters the location of membrane proteins such as β-integrins (*8, 9*), alters cell metabolism, induces DNA damage, and ultimately leads to cell death if the injury is sustained *(*10*).* Tubular cells surviving after AKI are largely responsible for repairing the kidney. These tubular cells undergo dedifferentiation and morphological changes, migrate along the basement membrane, proliferate, and finally differentiate to restore a functional nephron (*11–14*). Recent evidence and the introduction of more sensitive kidney injury

markers have challenged the paradigm that repair is without consequences, demonstrating that, in many cases, the extraordinary ability of the kidney to repair is incomplete, and AKI leads to maladaptive repair with persistent parenchymal inflammation, pericyte/fibroblast proliferation, and excessive deposition of extracellular matrix *(*10*).* We have reported that severe AKI leads to tubular cell cycle arrest in the G_2-M phase of the cell cycle with secretion of profibrotic factors at least partially mediated by c-Jun N-terminal kinase (JNK) signaling (2). However, the exact cellular mechanisms involved in secretion of profibrotic factors in G_2-M–arrested cells are not well understood.

Senescence is a state characterized by chromatin reorganization, cell cycle exit, and the secretion of the senescence-messaging secretome, which includes inflammatory cytokines, modulators of the extracellular matrix, and growth factors *(*15*).* Recently, a new compartment of the senescent cell has been described, named the target of rapamycin (TOR)–autophagy spatial coupling compartment (TASCC) (16). The TASCC forms from the association of the late autophagosome and the mammalian TOR complex 1 (mTORC1) kinase with the exclusion of Unc-51–like kinase 1 (16). Organelles are degraded in autophagosomes, releasing amino acids that induce the movement of mTORC1 to the lysosomal membrane *(*17*).* The Ragulator complex interacts with Rag guanosine triphosphatases (GTPases) and tethers Rag heterodimers to the lysosome. The complex is critical for TORC1 kinase activation through Rheb, resulting in increased endoplasmic reticulum (ER)–mediated protein synthesis and increased secretion of proteins (*16, 17*). Enhanced protein synthesis increases lysosomal and other membrane proteins, which can refuel the TASCC, leading to a vicious circle. This tightly regulated process is sensitive to any intervention that will disrupt amino acid flux or the localization of mTORC1 to the TASCC (16). The TASCC structure has been observed in kidney podocytes (16), but neither its presence nor its role in pathophysiological states in vivo has been described. We hypothesized that the TASCC plays a crucial role in the secretion of profibrotic factors by G_2-M–arrested PTCs.

RESULTS

TASCC formation is observed in PTCs during kidney fibrosis progression

To investigate whether TASCC formation was involved in the development and/or progression of CKD after AKI, we performed several models of AKI in mice leading to various degrees of fibrosis. As we have previously reported (2), aristolochic acid (AA) injection (5 mg/kg body weight), 32 min of bilateral renal ischemia reperfusion injury (IRI), or 30 min of unilateral renal IRI (UIRI) led to severe fibrosis in BALB/c mice (Fig. 1A) 21 days after injury. We first explored whether TASCC formation occurred in our models by staining with mTOR, LC3, and LAMP2 antibodies. Whereas TASCC structures were almost undetectable in tubule cells from sham-treated mice (Fig. 1, A and B), many TASCCs were seen in tubular sections after severe kidney injury (Fig. 1, A and B). TASCC structures, as shown previously in a lung fibroblast cell line *(*16*),* were also positive for p62 (fig. S1A). Using colocalization experiments with *Lotus tetragonolobus* agglutinin (LTA), a specific marker of differentiated PTCs, and mTOR, we found that TASCCs were mainly expressed in PTCs (Fig. 1C). To better understand the development of TASCC during CKD, we

performed a time course using different models of injury. During the acute phase of injury, at days 2 and 7, there was no statistically significant increase in $TASCC^+$ cells (Fig. 1D). The number of tubular cells expressing TASCC increased progressively starting after day 7 to day 21 after injury and remained high on day 42 (Fig. 1D) in the three models, AA, severe IRI, and UIRI, that are associated with greater degrees of fibrosis. We confirmed the specificity of our primary antibodies for TASCC components by performing the same experiment with isotype-matched immunoglobulin G (IgG) from each species used in the study (fig. S1B).

To better understand the relationship between $TASCC^+$ cells and the extent of fibrosis, we included an additional model of AKI that led to less fibrosis (moderate IRI, 30 min of ischemia), and two rescue models of fibrosis (2) including UIRI followed 3 days later by a contralateral nephrectomy, and mice with UIRI that were treated with pifithrin-α (PIF-α) injection, a p53 inhibitor (Fig. 1, A and D, and fig. S1C). TASCCs were seen in PTCs in both models, but fewer were present when compared to severe injury models, which lead to more fibrosis (Fig. 1, A and D, and fig. S1C).

PTCs arrested in G_2-M of the cell cycle stain positive for TASCC

We next investigated whether TASCC formation was present in G_2-M–arrested proximal tubule cells involved in fibrosis progression (2). We costained cells with phospho-H3 (pH3) antibody, as a marker of the G_2-M phase (2), and mTOR antibody (Fig. 2A). As we previously reported (2), AA injection and severe bilateral or unilateral IRI lead to an increased number of $pH3^+$ cells. After AA injection, there were fewer $pH3^+$ cells with mTOR staining characteristic of TASCC formation early after AA injection but the number increased progressively so that up to 80% of $pH3^+$ cells on day 42 after injection were also $TASCC^+$ (Fig. 2, A and B). Most of the tubular cells (85%) with mTOR distribution consistent with TASCC formation expressed pH3 (Fig. 2C).

To further characterize the relationship between the G_2-M phase of the cell cycle and TASCC formation, we treated two cell lines with characteristics of the proximal tubule, HK-2 and LLC-PK1 cells, with AA. After 48 hours of AA treatment, mTOR and LC3 distribution in the cell was reorganized from a diffuse location to specific punctate regions of the cell typical of a TASCC in both LLC-PK1 cells (Fig. 2, D and E) and HK-2 cells (fig. S1D). Western blot analysis revealed an increase in the membrane accumulation of LC3 in AA-treated LLC-PK1 (Fig. 2F and fig. S1D). To determine the stage of autophagosome maturation in which LC3 was associated with TASCC structures, we transfected ptf-LC3 [encoding a pH-sensitive green fluorescent protein (GFP) and pH-resistant red fluorescent protein (RFP) tagged to LC3 (18)] and treated with AA. TASCC structures, LC3 and mTOR positive, were found to be associated with the RFP, indicating late autophagosomes that have fused with lysosomes (Fig. 2G). Together, these data suggest that TASCC formation occurs in PTCs arrested in the G_2-M transition.

We evaluated the link between DNA damage, G_2-M cell cycle phase, and TASCC formation. We first confirmed, using phosphorylated H2AX (γH2AX) immunostaining, that AA induced DNA damage (Fig. 2H). Most of the cells with DNA damage expressed LC3 in a TASCC pattern (Fig. 2H, right panel). With DNA damage, coimmunostaining experiments

with pH3, mTOR, and LAMP2 revealed that most of the $pH3^+$ cells contained relocalized mTOR and LAMP2 in TASCCs (Fig. 2I and fig. S1E). Western blot analysis of the supernatant showed that LLC-PK1 and HK-2 cells treated with AA secreted the profibrotic factor, connective tissue growth factor (CTGF), into the culture medium (Fig. 2J). Thus, PTCs in the G_2-M phase of the cell cycle after injury express TASCC and secrete the profibrotic factor CTGF.

Cyclin G1 is a key factor during G_2-M arrest and TASCC formation

To elucidate the molecular pathways of G_2-M arrest and TASCC formation induced by AA, we performed an unbiased profiling of gene expression data (fig. S2A). We interrogated microarray data comparing the complementary DNA profiles in the kidneys of rats administered either vehicle or AA (10 mg/kg), five times per week by oral gavage, for 12 weeks *(*19*).* RNA was isolated and compared across five different microarray platforms (Affymetrix 1, 2, GE Healthcare, ABI, and Agilent) from Gene Expression Omnibus (GEO) (series accession number GSE5350). We found 47 genes whose expression differed significantly on all platforms after AA injection *(*$P < 0.001$) (19). Grouping these results by gene ontology category, we observed a range of functions for the 47 transcripts, including cell cycle–apoptosis, development, metabolism, and cell proliferation. Ingenuity Pathway Analysis (IPA) revealed that the top two pathways up-regulated by AA were the glutathione detoxification pathway and the p53 pathway (fig. S2B). Previously, we reported that the p53 pathway contributes to G_2-M arrest and fibrosis in several animal models of kidney fibrosis *(*2*).* The p53 pathway genes most highly up-regulated in this study were *CDKN1A* (p21), *BBC3* (PUMA), and *Ccng1* (cyclin G1) (fig. S2B). Of these, cyclin G1 is known to directly regulate G_2-M arrest *(*20*).*

Cyclin G1 (CG1) is an atypical cyclin, regulated at the transcriptional level by p53, whose functions have not been clearly elucidated. CG1 is involved in the arrest of cell cycle progression through G_2-M phase and is induced by DNA damage (*20, 21*). Western blot analysis confirmed at the protein level the dramatic increase of CG1 21 days after injury induced either by AA or by severe bilateral or unilateral IRI (Fig. 3A). Animal models in which kidney fibrosis had been mitigated through p53 inhibition (UIRI + PIF-α) or through removal of the contralateral kidney after UIRI (UIRI + Nx day 3) had lower expression of CG1 (Fig. 3A). To better understand its role, we then imaged the colocalization of CG1, pH3, and LAMP2 in damaged kidneys. CG1 was mainly expressed in proximal tubule cells that were $pH3^+$, and $CG1^+$ cells also correlated with LAMP2 staining, consistent with TASCC formation (Fig. 3B). To corroborate our findings, we performed experiments in vitro, treating HK-2 cells with AA. AA induced the expression of CG1 in G_2-M phase cells (Fig. 3C).

To further decipher the relationship between CG1, G_2-M arrest, and TASCC formation, we transfected HK-2 cells with CG1 (Fig. 3D). Transfection of either mCG1 or hCG1 induced a higher percentage of $pH3^+$ G_2-M phase cells (fig. S3, A and B). To test whether CG1 induced G_2-M arrest directly, we transfected LLC-PK1 cells with CG1, pulsed with 5-bromo-2′-deoxyuridine (BrdU) for 3 hours, and fixed cells 8 hours after the pulse. We found that the number of cells double positive for BrdU and pH3 after the pulse chase was

significantly increased in hCG1-transfected cells ($P = 0.0013$) (Fig. 3E). $pH3^+$ CG1-transfected cells also stained positive for TASCC (mTOR and LAMP2) (Fig. 3F). In addition, transfection with CG1 led to an increased production of profibrotic cytokines, including transforming growth factor–β1 (TGF-β1) in cell lysates (Fig. 3G and fig. S3C), and CTGF secretion into supernatants (Fig. 3H), even in the absence of the CG1 regulator p53 (Fig. 3I). The production of TGF-β1 was enhanced by sublethal injury with AA (10 μg/ml) but not with lethal injury via AA (20 μg/ml) (Fig. 3G). Thus, CG1 plays a role in increasing the number of cells in G_2-M, TASCC formation, and profibrotic factor production/secretion.

CG1 and TASCC are increased in G_2-M phase cells in a model of liver fibrosis

To determine whether the increases in CG1 and TASCC formation were specific for kidney fibrosis progression, we administered vehicle (mineral oil) or carbon tetrachloride (CCl_4) to mice three times per week for 12 weeks. CCl_4 is a toxin well known to induce liver fibrosis (22). As expected, CCl_4 administration was associated with the development of liver fibrosis, particularly surrounding the central vein (Fig. 4A). CCl_4 administration was associated with a greater number of $pH3^+$ cells compared to vehicle-treated animals (Fig. 4, B and D). Whereas $TASCC^+$ cells were barely detectable in the liver of the vehicle-treated group, about 55% of the $pH3^+$ cells were also $TASCC^+$ after CCl4 administration (Fig. 4, B and D). Furthermore, whereas CG1 was not detectable in the liver of the vehicle-treated group, it was induced in the liver after CCl4 administration and colocalized with $TASCC^+$ G_2-M phase cells (Fig. 4, C and D). Hence, increased CG1 expression is associated with an increase in the number of G_2-M phase cells, TASCC formation, and liver fibrosis.

CG1 and G_2-M arrest promote PTC dedifferentiation

G_2-M arrest is associated with a number of phenotypes, including dedifferentiation, senescent-like changes, cell size changes, and increased secretion of proinflammatory and profibrotic cytokines in kidney cells as well as other cell types (*23–25*). To determine whether CG1-associated G_2-M arrest promotes dedifferentiation phenotypes, we analyzed differentiation markers in LLC-PK1 cells treated with AA or transfected with CG1. AA treatment induced an increase in cell size (fig. S3, D and E), significantly reduced ZO-1 expression in LLC-PK1 cells, and promoted vimentin expression (fig. S3F). *hCG1* transfection led to decreased expression of Na/K-ATPase (adenosine triphosphatase), which is normally highly expressed in PTCs (Fig. 5A), and increased expression of vimentin, when combined with AA treatment (Fig. 5B). These data suggest that AA- or CG1-induced cell cycle changes promote dedifferentiation of PTCs. To test whether CG1 induced a senescent-like state, we tested whether CG1 knockout reduced β-galactosidase (β-gal) activity. Wild-type mouse primary PTCs treated with AA demonstrated an about fivefold increase in β-gal staining compared to wild-type cells treated with PBS. $CG1^{-/-}$ cells had no increase in β-gal staining with AA treatment (Fig. 5C).

Preventing TASCC formation reduces profibrotic factor secretion

Next, we determined whether targeting TASCC activity could decrease fibrosis. In response to amino acid release, mTORC1 is recruited to the membrane of the lysosome through the Rag GTPase complex (*26, 27*). Dominant negative forms of Rag GTPase can disrupt the

recruitment of mTORC1 to the lysosome upon amino acid stimulation (*26, 27*). A dominant negative form of *RagB* has been shown to disrupt the recruitment of mTORC1 to the TASCC and reduce interleukin-6/8 production in oncogene-induced senescence cells (16). To explore the relevance of these findings to our models, we transfected LLC-PK1 cells with EV, *hCG1,* the dominant negative form of *RagB* (RagB DN), or *hCG1* + *RagB* DN and exposed them to AA. LLC-PK1 cells transfected with EV and exposed to AA secreted CTGF (Fig. 5D). LLC-PK1 cells transfected with *hCG1* spontaneously secreted CTGF (Fig. 5D). Transfection of LLC-PK1 cells with *hCG1* increased the number of cells in the G_2-M phase of the cell cycle (Fig. 5E). LLC-PK1 cells transfected with the *RagB* DN secreted less CTGF in response to AA (Fig. 5D). To further characterize the role of CG1 during TASCC formation, we cotransfected LLC-PK1 cells with *hCG1* and *RagB* DN and exposed cells to AA or diluent. Although there was an increase in the number of cells in G_2-M, the cotransfected cells *(hCG1* + *RagB* DN) treated with AA produced less CTGF when compared to cells treated with EV (Fig. 5, D and E). Coimmunostaining experiments revealed that LLC-PK1 cells transfected with *RagB* DN and exposed to AA did not form TASCC (Fig. 5, F and G). Thus, mTORC1 recruitment was important for the production of TASCC in cells treated with AA. In addition, these experiments suggest that targeting the TASCC would reduce fibrotic factor synthesis.

TASCC blockade is protective against fibrosis progression

Next, we tested whether targeting the TASCC in vivo could be a potential therapeutic approach to prevent kidney fibrosis progression. Rapamycin or everolimus, two mTOR inhibitors, have been reported to either exacerbate *(28, 29)* or improve *(30–32)* fibrosis and tubular dilation in different mouse models of CKD. Introducing these inhibitors early after the injury (28) is associated with worsening kidney lesions, whereas administration later is associated with improvement of fibrosis and tubular dilation (*30, 32*). We hypothesized that rapamycin would interfere with normal repair when they are injected early after injury, whereas their injection later would target both mTORC1 and mTORC2 and hence inhibit TASCC formation in G_2-M cells (*33–35*).

To avoid potential complications with small molecule inhibitors, we used a genetic approach to specifically block TASCC formation in the proximal tubule after injury. Raptor is a major component of the mTOR complex 1. We bred $Raptor^{flox/flox}$ mice with *Slc34a1*-GFPCreER^{T2} $(Slc34a1^{GCE/+})$ mice to generate $Slca341^{GCE/+}$; $Raptor^{flox/flox}$ mice, which, upon tamoxifen administration (36), lack raptor expression in the proximal tubule (hereafter identified as $Raptor^{\Delta PT}$*).* $Slca341^{GCE/+}$; $Raptor^{flox/flox}$ mice not treated with tamoxifen are designated $Raptor^{flox/flox}$. Prolonged bilateral renal IRI (32 min) was carried out in mice with or without tamoxifen injection (3 doses every other day) to induce *Cre* expression initiated either 7 days before injury or day initiated 21 after injury, and examined tissue 42 days after injury. We first confirmed that *Cre* recombination was efficient in reducing raptor expression in the kidney cortex by immunocytochemistry, confirming deletion of raptor in most of the LTA$^+$ PTCs (Fig. 6A). Western blot analysis of whole-kidney lysates revealed significantly less raptor expression after *Cre* recombination ($P < 0.001$) (Fig. 6B). $Raptor^{\Delta PT}$ mice with Cre recombination 7 days before IRI had worse kidney function with higher blood urea nitrogen (BUN) values at day 42 (Fig. 6C). However, $Raptor^{\Delta PT}$ mice with Cre

recombination initiated 21 days after IRI had a significantly lower BUN at 42 days after injury compared to either *Raptor*$^{flox/flox}$ ($P < 0.001$) or *Raptor*$^{\Delta PT}$ d−7 mice treated with Cre recombination 7 days before IRI ($P < 0.001$). Consistently, *Raptor*$^{\Delta PT}$ mice with Cre recombination 21 days after IRI had a lower expression of fibrosis markers [α-smooth muscle actin (αSMA), fibronectin, and COL4A1 mRNA] and less fibrosis as assessed histologically (Fig. 6, D to F). Coimmunostaining experiments in tissue from mice sacrificed on day 42 after renal IRI showed fewer TASCCs in *Raptor*$^{\Delta PT}$ d+21 mice compared with the control wild-type *Raptor*$^{flox/flox}$ mice not treated with tamoxifen (fig. S4, A and B). As expected, the percentages of PTCs staining for BrdU and pH3 were similar in the two groups of mice, indicating that disrupting Raptor did not alter G_2-M arrest (fig. S4C). Likewise, we observed an up-regulation of CG1 expression in both *Raptor*$^{flox/flox}$ and *Raptor*$^{\Delta PT}$ after IRI, again demonstrating that loss of Raptor did not interfere with upstream signaling pathways, which promote G_2-M arrest (fig. S4D); there was, however, a dramatic reduction in the percentage of G_2-M cells (pH3) with TASCC structures (19% versus 79%) in the *Raptor*$^{\Delta PT}$ d+21 when compared to *Raptor*$^{flox/flox}$ mice (fig. S4, B and C).

We then investigated whether these findings were applicable to another model of chronic kidney injury. To this aim, we injected AA to *Raptor*$^{flox/flox}$ or *Raptor*$^{\Delta PT}$ mice and induced Cre recombination 21 days after the last AA injection. Consistent with results in the IRI model, *Raptor*$^{\Delta PT}$ mice with Cre recombination on day 21 after injury had a lower BUN 39 days after AA administration compared to *Raptor*$^{flox/flox}$ mice (Fig. 6G), reduced expression of fibrotic markers, and a lower kidney fibrosis score (Fig. 6, H to J). These data show that inhibition of the formation of TASCC in PTCs in vivo reduces kidney fibrosis progression after injury.

Deletion of CG1 inhibits TASCC formation and fibrosis

To determine the role of CG1 in kidney fibrosis progression, we induced kidney injury in CG1$^{-/-}$ mice by AA injection and monitored TASCC formation and kidney fibrosis 6 weeks after injection. CG1$^{-/-}$ mice had reduced protein expression of the kidney injury marker KIM-1 6 weeks after AA injection (Fig. 7, A and B). As expected, CG1$^{-/-}$ mice also had a reduced percentage of pH3^{+} G_2-M phase cells (Fig. 7C). Kidney injury, as measured by serum creatinine, was similar between wild-type and CG1 knockout mice during the acute phase of injury (Fig. 7D). Next, we analyzed TASCC formation in CG1$^{-/-}$ mice by quantifying the colocalization of LC3, LAMP2, and mTOR using Pearson's correlation. TASCC formation was significantly reduced in kidneys from CG1$^{-/-}$ compared to wild-type mice ($P < 0.05$) (Fig. 7, E and F). With AA treatment, kidney fibrosis was about 50% less in CG1$^{-/-}$ mice compared to wild-type mice, as measured by quantification of polarized images of picrosirius red and Masson's trichrome stainings (Fig. 7, G to I). CG1$^{-/-}$ mice also had reduced αSMA, TGF-β, and CTGF mRNA after AA-induced injury (Fig. 7, J to L). These data indicate that CG1 regulates G_2-M arrest and subsequent TASCC formation in vivo, ultimately contributing to kidney fibrosis progression.

TASCC formation is increased in G_2-M phase cells in patients with CKD

We evaluated the relevance of our findings using tissue samples from 5 control patients, 10 with AKI, and 40 with CKD of various etiologies including chronic interstitial nephritis (n =

10), AA nephropathy (n = 10), diabetic kidney disease (DKD) (n = 10), and hypertension nephropathy (n = 10) (table S1). Using colocalization studies on human kidney biopsy tissue, we quantitated the number of tubular cells that contained TASCC per field (40×) (Fig. 8, A and B) and the number of $pH3^+$ tubular cells that contained TASCC per 40× field (Fig. 8, C and D and fig. S5) and compared the findings to controls (n = 5). TASCC formation was enriched in cells in the G_2-M phase of the cell cycle in each of the disease groups (Fig. 8D). There was a correlation between $TASCC^+$ tubular cells and fibrosis (R^2 = 0.615, P = 0.008) but not with urine albumin/creatinine ratio (fig. S5, B and C).

DISCUSSION

By combining several experimental models of AKI to CKD transition in mice, studies with epithelial cells in vitro, unbiased gene expression analyses and validation in human biopsies, we identified a mechanism of kidney fibrosis development and progression. As we previously reported, after injury that ultimately leads to fibrosis, a certain percentage of PTCs are arrested in the G_2-M phase of the cell cycle (2). These cells participate in maladaptive repair by secreting profibrotic factors with potential auto- and paracrine effects. Here, we show that CG1 induction is sufficient to increase the number of cells in the G_2-M phase and that a high percentage of cells in the G_2-M phase have TASCCs, structures previously described in Ras-induced senescent cells *(*16*).* Inhibition of TASCC formation results in less kidney fibrosis after injury, thus identifying a potential new therapeutic target. Furthermore, we confirmed that these findings are relevant to human CKD.

Our study reveals that increased TASCC formation is associated with synthesis and secretion of profibrotic factors, similar to the senescence-messaging secretome, leading to fibrosis and its progression. Secreted factors may potentiate cell cycle arrest in G_2-M (*2,* 24*).* Some tubular cells expressing the TASCC were not in G_2-M, but were in the close vicinity of $pH3^+$ cells. These results are in accordance with recent findings showing that the senescence of one cell can be transmitted by secretory paracrine mechanisms to neighboring cells (37).

We found that TASCC formation was mediated through CG1 induction. CG1 is an atypical cyclin whose precise roles are unknown. It interacts with p53 and p21, two cyclin-dependent kinase inhibitors playing a role in G_2-M arrest and kidney fibrosis progression (2, *38–41).* CG1 is induced by DNA damage (42) and promotes G_2-M arrest *(20, 43).* In kidney epithelial cells in culture, the overexpression of *cyclin G1* was sufficient to induce G_2-M arrest, TASCC formation, and profibrotic factor secretion. Deletion of CG1 prevented G_2-M arrest, inhibited TASCC formation, and reduced kidney fibrosis after injury. Although CG1 was up-regulated and there was an increased number of cells at the G_2-M transition in the cell cycle in $Raptor^{\Delta PT}$ mice after IRI, TASCC formation was not detectable and fibrosis was reduced, reinforcing that the profibrotic events downstream of CG1-facilitated G_2-M arrest are mediated by TASCC formation. Furthermore, we demonstrated that this process is not unique to the kidney and may represent a common process of fibrosis progression, because it was also detectable in fibrotic liver.

AKI is marked by dramatic injury and loss of kidney tubular cells, especially in the proximal tubule. As part of this repair process after kidney injury, it is known that PTCs undergo

dedifferentiation to migrate, alter their morphology, and divide to reform the damaged tubule segments *(9, 11, 12, 14, 24, 44, 45).* We found evidence of increased cell size, reduced differentiation marker expression, increased dedifferentiation marker (vimentin), and increased senescence in PTCs overexpressing CG1 or treated with AA. It is particularly interesting that CG1 overexpression alone mimicked dedifferentiation characteristics observed in injured PTCs and enhanced the effects of injury on dedifferentiation. It is unlikely that CG1-induced G_2-M arrest regulates dedifferentiation, because PTCs must dedifferentiate early in the process of entering the cell cycle. CG1 has been reported to regulate epithelial-mesenchymal transition (EMT) in hepatocellular carcinoma cell lines through SNAIL stabilization (46). Together, these data suggest a role for CG1 expression in regulating the dedifferentiation status of PTCs.

TASCC blockade is sufficient to reduce the severity of kidney fibrosis progression. In vitro, we confirmed that cells transfected with a dominant negative *RagB* construct have reduced synthesis of fibrotic factors. Dominant negative *RagB* is not able to recruit mTORC1 to the lysosome membrane, preventing TASCC formation. In vivo, genetic deletion of raptor in PTCs, performed 21 days after bilateral IRI, reduced the kidney fibrosis score 42 days after IRI. This may explain the apparent discrepancy of the impact of mTORC inhibitor administration in mouse models of nephron reduction *(28).* Exposure to mTORC inhibitors early after injury leads to severe renal lesions related to inhibition of the normal repair process (28), whereas late administration improves kidney lesions *(30, 32),* potentially due to TASCC blockade and inhibition of secretion of profibrotic growth factors and cytokines in G_2-M–arrested cells involved in the maladaptive repair.

TASCC formation was also seen in humans with kidney disease. We studied a group of patients with various causes of CKD that developed progressive fibrotic lesions. Compared to controls, kidney tissue with fibrosis contained more PTCs in the G_2-M phase of the cell cycle, and these cells expressed TASCCs. We also found $TASCC^+$ cells in patients with AKI. Although the biopsies are from patients with AKI, they can be expected to be derived at varying times after the initiation of the insult or insults and most patients with AKI will have some degree of underlying CKD or progress to CKD.

In conclusion, we have identified a mechanism of fibrosis progression involving the induction of CG1-promoted TASCC formation, which facilitates profibrotic factor secretion in cells in the G_2-M phase of the cell cycle. This pathway may represent a new promising therapeutic target.

MATERIALS AND METHODS

Study design

The objective of this study was to determine the underlying cause of G_2-M arrest and profibrotic secretory phenotypes in kidney epithelial cells that promote kidney fibrosis. Using a systems biology approach, we identified the p53 pathway, and in particular CG1, as the most likely pathway regulating G_2-M arrest and senescence-like phenotypes in kidney fibrosis. We hypothesized that CG1 induces G_2-M arrest in kidney tubule epithelial cells, contributing to (senescence-associated) TASCC formation and secretion of profibrotic

cytokines. To test this hypothesis, we designed a study using human tissue, multiple models of kidney injury in normal mice, mice deficient in CG1 or components of the TASCC, and in vitro models of tubular cell injury to determine the role of CG1 and TASCC in CKD. We selected sample sizes to have 80% power to detect a 50% reduction in fibrotic area (as calculated by power analysis using Student's *t* test) based on data from wild-type mice and past experience with models of kidney injury in mice. Inclusion/exclusion criteria were kept to a minimum and established before any quantification. For animal studies, as much as possible, we used littermates, which facilitates appropriate randomization. Within the littermate groups, animals were selected at random for IRI or sham surgeries. The IRI surgery was performed by an investigator who was not aware of the genotype or experimental assays to be performed after the surgery. For studies with AA, animals from each genotype were chosen at random, within littermates, for the vehicle or treatment groups. For in vitro studies, a minimum of three experimental replicates was performed. The number of replicates is indicated in the figure legends. For all cell experiments in vitro, equal numbers of cells were plated. Processing was performed simultaneously and in parallel for all conditions within each experiment. Human samples were carefully evaluated by two independent pathologists. Statistical tests were chosen based on nature of variables, assumption of data distribution, and effect size. In general, continuous data were analyzed by Student's *t* test, Mann-Whitney test, or ANOVA. False discovery rate was controlled by conducting at least three independent experiments. In the case of multiple comparisons, Tukey's post hoc test was used. Primary data are reported in data file S1.

Animals

Kidney models of injury—Mice were male BALB/c and C57BL/6 mice, aged 8 to 10 weeks (20 to 22 g), purchased from Charles River Laboratories. Raptor$^{flox/flox}$ mice on a C57BL/6 background were purchased from the Jackson Laboratory. CG1$^{-/-}$ mice were provided by S. Thorgeirsson at the National Cancer Institute, National Institutes of Health, USA.

Ischemia was induced by the retroperitoneal approach on both kidneys for 30 min at 37.0°C (moderate IRI, $n = 24$ mice) or for 32 min at 37.5°C (severe IRI, $n = 24$) or only the left kidney for 30 min at 37°C (unilateral IRI, $n = 24$) in BALB/c mice, as previously reported *(2).* For the UIRI model, two approaches were taken in several groups of mice: Nephrectomy of the contralateral kidney was performed 3 days after UIRI surgery ($n = 24$ mice) or mice were given PIF-α (2.2 mg/kg body weight, Sigma), dissolved in phosphate-buffered saline (PBS), intraperitoneally on days 3 and 14 after UIRI surgery ($n = 24$). PBS was injected in the control groups. One milliliter of warm saline (37°C) was injected intraperitoneally after all surgeries for volume supplement. Sham operations were performed with exposure of both kidneys but without induction of ischemia. AAN was induced in BALB/c mice by a one-time intraperitoneal injection of AA (5 mg/kg body weight, Sigma) in PBS ($n = 36$ mice). The normal control mice were administered the same amount of PBS ($n = 24$).

Conditional Raptor knockout—*Raptor$^{flox/flox}$* mice were crossed with *Slc34A1.CreER^{T2}* mice to generate specific proximal tubule cells *Raptor* knockout mice *(Raptor$^{\Delta PT}$)* on the C57BL/6 background (36). Ischemia (26-min) reperfusion injury was

performed on 12 control wild-type *Slc34a1*$^{GCE/+}$; *Raptor*$^{flox/flox}$ (*Raptor*$^{flox/flox}$) and 12 *Raptor*$^{\Delta PT}$ adult (8- to 10-week-old) mice. Cre recombinase was induced either 7 days before ischemia or on day 21 after IRI by intraperitoneal injection of tamoxifen (300 μg, Sigma-Aldrich) to mice every other day, for a total of three times. Deletion using Slc34A1$^{CGE/+}$ has been shown to occur within 1 week of tamoxifen injection (36). Tamoxifen (Sigma-Aldrich) was dissolved in 3% (v/v) ethanol containing corn oil (Sigma-Aldrich). *Slc34a1GCE* expression was up-regulated before tamoxifen injection by feeding mice a low-phosphorus (0.06%) diet (TestDiet) (36). In all cases, littermate control phenotypes were compared.

AA injury was induced in 10- to 12-week-old male Raptor $^{flox/flox}$ and Raptor $^{flox/flox}$:SLC34a1GCE mice or CG1$^{-/-}$ and wild-type mice which are on a C57BL/6 background. AA (Sigma) was administered to mice intraperitoneally (3 mg/kg body weight) every other day for three times. Eleven days after the last dose of AA injection, three doses of tamoxifen (300 μg) were injected every other day (36). Mice were sacrificed 5 weeks after the last dose of AA.

Animals were fed ad libitum and housed at constant ambient temperature in a 12-hour light cycle. All animal experiments were performed in accordance with the animal use protocol approved by the Institutional Animal Care and User Committee of Harvard Medical School, the Institutional Animal Care and User Committee of Vanderbilt University Medical Center, and the Institutional Review Board of Tokushima University Graduate School for Animal Protection.

Liver models of injury—C57BL/6 male mice received either vehicle (mineral oil) or CCl_4 (Sigma) (n = 6 mice per group) by oral gavage three times per week for 12 weeks according to an escalating dose protocol (first dose, 0.875 ml/kg; weeks 1 to 3, 1.75 ml/kg; weeks 4 to 6, 2.5 ml/kg; weeks 7 to 12, 3.25 ml/kg) as previously described (47).

Cell culture

The HK-2 (human) and LLC-PK1 (pig) proximal cell lines were cultured in DMEM (Dulbecco's modified Eagle's medium) supplemented with 10% fetal calf serum (FCS) until the cells were 80% confluent. Cells were then incubated in DMEM containing 0.2% FCS for 24 hours. After growth factor deprivation, cells were treated with AA (5–20 μg/ml) in full medium (DMEM with 10% FCS) for 48 hours. Conditioned medium was then collected, and the cells were collected by either trypsinization, for flow cytometry, or lysed in 1× sample buffer [50 mM tris-HCl (pH 6.8), 10% glycerol, 2% SDS, and 12.5 mM EDTA] for immunoblot analysis.

Immunofluorescence

Cultured cells were fixed in 4% paraformaldehyde for 20 min, permeabilized in PBS containing 0.2% Triton X-100 and 3% bovine serum albumin, and incubated with primary antibodies to the indicated protein of interest, followed by Alexa Fluor–conjugated secondary antibodies (Jackson ImmunoResearch).

For human kidney biopsies and mouse kidney samples, 4-pm sections of paraffin-embedded kidneys were submitted to antigen retrieval protocols using high temperature (120°C) and high pressure in citrate buffer and a pressure cooker. Sections were then incubated with primary antibodies as indicated and appropriate Alexa Fluor-conjugated secondary antibodies (Jackson ImmunoResearch). Immunofluorescence for human tissue was performed on $n = 10$ kidney tissue per group of renal disease and $n = 5$ controls. The control group was composed of healthy renal peritumoral tissues. Renal function and albumin/creatinine ratio were determined at the time of biopsy.

Fibrosis quantification

Kidney sections were stained with Masson's trichrome or picrosirius red and quantified using Nikon NIS Elements software or scored by an experienced pathologist in a blinded manner. Briefly, mouse kidney sections were stained using Masson's trichrome, a mixture of three dyes including aniline blue that is specific to collagen fibers, at the Brigham and Women's Hospital Pathology Core *(48).* The collagen-positive area was quantified using NIS Elements software. Other mouse kidney sections were stained with picrosirius red (EMS) using the manufacturer's protocol, and whole-kidney sections were imaged at ×10 magnification, stitched images, under polarized light. Positive area was quantified using NIS Elements software. Picrosirius red staining binds specifically to collagen and increases the birefringence properties of the collagen fibers, when observed by polarized light microscopy *(49).* The renal papilla was omitted from quantification as it contains collagen-rich vascular structures, which skew the results. Human kidney samples were assessed using trichrome staining. The slides were reviewed in a blinded manner by two pathologists and were graded using quantitative image analysis. Results were expressed as a percentage of fibrosis and scored (grade I, <25%; grade II, 26 to 50%; grade III, >50%).

Antibodies

The following primary antibodies were used for immunofluorescence or Western blot.

Immunofluorescence: mTOR (Cell Signaling Technology, rabbit, 1:50), LC3 (Nanotools, mouse, 1:50), LAMP2 (Developmental Studies Hybridoma Bank at the University of Iowa, rat, GL2A7, 1:25), vimentin (Developmental Studies Hybridoma Bank at the University of Iowa, mouse, 1:50), CG1 (Santa Cruz Biotechnology, rabbit, 1:50), LTA (Vector Laboratories), Ki-67 (Vector Laboratories, rabbit, 1:50), and pH3 (Cell Signaling Technology, mouse, 1:50).

Western blot: CTGF-specific antibody (GeneTex, 1:1000), rabbit antibody to CG1 (Santa Cruz Biotechnology, 1:500), mouse antibody to LC3 (Nanotools, 1:500), rabbit antibody to extracellular signal-regulated kinase (ERK) (Cell Signaling, 1:1000), rabbit antibody to Raptor (Cell Signaling, 1:500), rabbit antibody to TGF-β (Cell Signaling, 1:500), Na^+/K^+-ATPase (Developmental Studies Hybridoma Bank at the University of Iowa, mouse, 1:50), and rabbit antibody to β-actin (Sigma, 1:5000).

Statistical analysis

Statistical analyses were performed using Prism 6.07 (GraphPad Software Inc.). All results are reported as means ± SEM. Statistical tests are two-tailed, unpaired Student's *t* tests and one-way ANOVA followed by Tukey's post hoc test. A P value of <0.05 was interpreted as statistically significant. In general, normal distribution was assumed with a sample size of $n > 30$. In case nonparametric test showed lack of power and robustness in a smaller sample size, parametric test and strict control of the false discovery rate were applied.

Supplementary Material

Refer to Web version on PubMed Central for supplementary material.

Acknowledgments

Funding: This work was supported by Safra Foundation and NIH grants R37DK039773 and R01DKD072381 (to J.V.B.); K01DK099473 and P30 DK114809 (to C.R.B.); Philippe Foundation Inc., Bettencourt Schueller Foundation, Société Française de Néphrologie, Emmanuel Boussard Foundation (London, UK), Day Solvay Foundation (Paris, France), Assistance Publique-Hôpitaux de Paris, and University Paris Descartes (to G.C.); and Research Fellowship from Sumitomo Life Welfare and Culture Foundation, Japan and Grant in Aid for Scientific Research (C; 16 K09620; to S.K.).

Competing interests: J.V.B. is a co-inventor on KIM-1 patents assigned to Partners Healthcare. He is an advisor for Boehringer Ingelheim, BioMarin, Takeda, and Lilly and receives grant support from Boehringer Ingelheim. He holds equity in Goldfinch Bio, Theravance, Sentien, and Rubius.

REFERENCES AND NOTES

1. Basile DP, Donohoe D, Roethe K, Osborn JL, Renal ischemic injury results in permanent damage to peritubular capillaries and influences long-term function. Am. J. Physiol. Renal Physiol 281, F887–F899 (2001). [PubMed: 11592947]
2. Yang L, Besschetnova TY, Brooks CR, Shah JV, Bonventre JV, Epithelial cell cycle arrest in G2/M mediates kidney fibrosis after injury. *Nat. Med.* 16, 535–543 (2010). [PubMed: 20436483]
3. Hsu C.-y., Yes, AKI truly leads to CKD. *J. Am.* Soc. *Nephrol.* 23, 967–969 (2012). [PubMed: 22499588]
4. Coca SG, Singanamala S, Parikh CR, Chronic kidney disease after acute kidney injury: A systematic review and meta-analysis. Kidney Int. 81, 442–448 (2012). [PubMed: 22113526]
5. Collins AJ, Foley RN, Chavers B, Gilbertson D, Herzog C, Johansen K, Kasiske B, Kutner N, Liu J, St Peter W, Guo H, Gustafson S, Heubner B, Lamb K, Li S, Li S, Peng Y, Qiu Y, Roberts T, Skeans M, Snyder J, Solid C, Thompson B, Wang C, Weinhandl E, Zaun D, Arko C, Chen SC, Daniels F, Ebben J, Frazier E, Hanzlik C, Johnson R, Sheets D, Wang X, Forrest B, Constantini E, Everson S, Eggers P, Agodoa L, United States Renal Data System 2011 Annual Data Report: Atlas of chronic kidney disease & end-stage renal disease in the United States. *Am. J. Kidney Dis.* 59, e1–420 (2012).
6. Go AS, Chertow GM, Fan D, McCulloch CE, C.-y. Hsu, Chronic kidney disease and the risks of death, cardiovascular events, and hospitalization. N. Engl. J. Med 351, 1296–1305 (2004). [PubMed: 15385656]
7. Sutton TA, Molitoris BA, Mechanisms of cellular injury in ischemic acute renal failure. Semin. Nephrol 18, 490–497 (1998). [PubMed: 9754601]
8. Gailit J, Colflesh D, Rabiner I, Simone J, Goligorsky MS, Redistribution and dysfunction of integrins in cultured renal epithelial cells exposed to oxidative stress. Am. J. Physiol 264, F149–F157 (1993). [PubMed: 8430825]
9. Zuk A, Bonventre JV, Brown D, Matlin KS, Polarity, integrin, and extracellular matrix dynamics in the postischemic rat kidney. Am. J. Physiol 275, C711–C731 (1998). [PubMed: 9730955]

10. Bonventre JV, Yang L, Cellular pathophysiology of ischemic acute kidney injury. J. Clin. Invest 121, 4210–4221 (2011). [PubMed: 22045571]
11. Bonventre JV, Dedifferentiation and proliferation of surviving epithelial cells in acute renal failure. J. Am. Soc. Nephrol 14, (suppl. 1), S55–S61 (2003). [PubMed: 12761240]
12. Humphreys BD, Valerius MT, Kobayashi A, Mugford JW, Soeung S, Duffield JS, McMahon AP, Bonventre JV, Intrinsic epithelial cells repair the kidney after injury. Cell Stem Cell 2, 284–291 (2008). [PubMed: 18371453]
13. Humphreys BD, Czerniak S, DiRocco DP, Hasnain W, Cheema R, Bonventre JV, Repair of injured proximal tubule does not involve specialized progenitors. Proc. Natl. Acad. Sci. U.S.A 108, 9226–9231 (2011). [PubMed: 21576461]
14. Canaud G, Bonventre JV, Cell cycle arrest and the evolution of chronic kidney disease from acute kidney injury. Nephrol. Dial. Transplant 30, 575–583 (2015). [PubMed: 25016609]
15. Campisi J, d'Adda di Fagagna F, Cellular senescence: When bad things happen to good cells. Nat. Rev. Mol. Cell Biol 8, 729–740 (2007). [PubMed: 17667954]
16. Narita M, Young ARJ, Arakawa S, Samarajiwa SA, Nakashima T, Yoshida S, Hong S, Berry LS, Reichelt S, Ferreira M, Tavare S, Inoki K, Shimizu S, Narita M, Spatial coupling of mTOR and autophagy augments secretory phenotypes. Science 332, 966–970 (2011). [PubMed: 21512002]
17. Zoncu R, Sabatini DM, The TASCC of secretion. Science 332, 923–925 (2011). [PubMed: 21596981]
18. Kimura S, Noda T, Yoshimori T, Dissection of the autophagosome maturation process by a novel reporter protein, tandem fluorescent-tagged LC3. Autophagy 3, 452–460 (2007). [PubMed: 17534139]
19. Guo L, Lobenhofer EK, Wang C, Shippy R, Harris SC, Zhang L, Mei N, Chen T, Herman D, Goodsaid FM, Hurban P, Phillips KL, Xu J, Deng X, Sun YA, Tong W, Dragan YP, Shi L, Rat toxicogenomic study reveals analytical consistency across microarray platforms. Nat. Biotechnol 24, 1162–1169 (2006). [PubMed: 17061323]
20. Kimura SH, Ikawa M, Ito A, Okabe M, Nojima H, Cyclin G1 is involved in G2/M arrest in response to DNA damage and in growth control after damage recovery. Oncogene 20, 3290–3300 (2001). [PubMed: 11423978]
21. Seo HR, Lee DH, Lee HJ, Baek M, Bae S, Soh JW, Lee SJ, Kim J, Lee YS, Cyclin G1 overcomes radiation-induced G2 arrest and increases cell death through transcriptional activation of cyclin B1. Cell Death Differ. 13, 1475–1484 (2006). [PubMed: 16322753]
22. Kuramitsu K, Sverdlov DY, Liu SB, Csizmadia E, Burkly L, Schuppan D, Hanto DW, Otterbein LE, Popov Y, Failure of fibrotic liver regeneration in mice is linked to a severe fibrogenic response driven by hepatic progenitor cell activation. Am. J. Pathol 183, 182–194 (2013). [PubMed: 23680654]
23. Blagosklonny MV, Cell cycle arrest is not yet senescence, which is not just cell cycle arrest: Terminology for TOR-driven aging. Aging 4, 159–165 (2012). [PubMed: 22394614]
24. Lovisa S, LeBleu VS, Tampe B, Sugimoto H, Vadnagara K, Carstens JL, Wu C-C, Hagos Y, Burckhardt BC, Pentcheva-Hoang T, Nischal H, Allison JP, Zeisberg M, Kalluri R, Epithelial-to-mesenchymal transition induces cell cycle arrest and parenchymal damage in renal fibrosis. Nat. Med 21,998–1009 (2015). [PubMed: 26236991]
25. Valentijn FA, Falke LL, Nguyen TQ, Goldschmeding R, Cellular senescence in the aging and diseased kidney. *J. Cell Commun. Signal.* 12, 69–82 (2018). [PubMed: 29260442]
26. Sancak Y, Peterson TR, Shaul YD, Lindquist RA, Thoreen CC, Bar-Peled L, Sabatini DM, The Rag GTPases bind raptor and mediate amino acid signaling to mTORC1. Science 320, 1496–1501 (2008). [PubMed: 18497260]
27. Sancak Y, Bar-Peled L, Zoncu R, Markhard AL, Nada S, Sabatini DM, Ragulator-Rag complex targets mTORC1 to the lysosomal surface and is necessary for its activation by amino acids. Cell 141, 290–303 (2010). [PubMed: 20381137]
28. Vogelbacher R, Wittmann S, Braun A, Daniel C, Hugo C, The mTOR inhibitor everolimus induces proteinuria and renal deterioration in the remnant kidney model in the rat. Transplantation 84, 1492–1499 (2007). [PubMed: 18091526]

29. Torras J, Herrero-Fresneda I, Gulias O, Flaquer M, Vidal A, Cruzado JM, Lloberas N, Franquesa M. l., Grinyo JM, Rapamycin has dual opposing effects on proteinuric experimental nephropathies: Is it a matter of podocyte damage? Nephrol. Dial. Transplant 24, 3632–3640 (2009). [PubMed: 19671594]
30. Diekmann F, Rovira J, Carreras J, Arellano EM, Banon-Maneus E, Ramirez-Bajo MJ, Gutierrez-Dalmau A, Brunet M, Campistol JM, Mammalian target of rapamycin inhibition halts the progression of proteinuria in a rat model of reduced renal mass. *J. Am. Soc. Nephrol.* 18, 2653–2660 (2007). [PubMed: 17804674]
31. Wu M-J, Wen M-C, Chiu Y-T, Chiou Y-Y, Shu K-H, Tang M-J, Rapamycin attenuates unilateral ureteral obstruction-induced renal fibrosis. Kidney Int. 69, 2029–2036 (2006). [PubMed: 16732193]
32. Kurdián M, Herrero-Fresneda I, Lloberas N, Gimenez-Bonafe P, Coria V, Grande MT, Boggia J, Malacrida L, Torras J, Arévalo MA, González-Martinez F, López-Novoa JM, Grinyó J, Noboa O, Delayed mTOR inhibition with low dose of everolimus reduces TGFβ expression, attenuates proteinuria and renal damage in the renal mass reduction model. PLOS ONE e32516, 7 (2012).
33. Sarbassov DD, Ali SM, Sengupta S, Sheen J-H, Hsu PP, Bagley AF, Markhard AL, Sabatini DM, Prolonged rapamycin treatment inhibits mTORC2 assembly and Akt/PKB. Mol. Cell 22, 159–168 (2006). [PubMed: 16603397]
34. Lamming DW, Ye L, Katajisto P, Goncalves MD, Saitoh M, Stevens DM, Davis JG, Salmon AB, Richardson A, Ahima RS, Guertin DA, Sabatini DM, Baur JA, Rapamycin-induced insulin resistance is mediated by mTORC2 loss and uncoupled from longevity. Science 335, 1638–1643 (2012). [PubMed: 22461615]
35. Canaud G, Bienaimé F, Viau A, Treins C, Baron W, Nguyen C, Burtin M, Berissi S, Giannakakis K, Muda AO, Zschiedrich S, Huber TB, Friedlander G, Legendre C, Pontoglio M, Pende M, Terzi F, AKT2 is essential to maintain podocyte viability and function during chronic kidney disease. *Nat. Med.* 19, 1288–1296 (2013). [PubMed: 24056770]
36. Kusaba T, Lalli M, Kramann R, Kobayashi A, Humphreys BD, Differentiated kidney epithelial cells repair injured proximal tubule. *Proc. Natl. Acad. Sci. U.S.A.* 111, 1527–1532 (2014). [PubMed: 24127583]
37. Acosta JC, Banito A, Wuestefeld T, Georgilis A, Janich P, Morton JP, Athineos D, Kang T-W, Lasitschka F, Andrulis M, Pascual G, Morris KJ, Khan S, Jin H, Dharmalingam G, Snijders AP, Carroll T, Capper D, Pritchard C, Inman GJ, Longerich T, Sansom OJ, Benitah SA, Zender L, Gil J, A complex secretory program orchestrated by the inflammasome controls paracrine senescence. *Nat. Cell Biol.* 15, 978–990 (2013). [PubMed: 23770676]
38. Sutton TA, Hato T, Mai E, Yoshimoto M, Kuehl S, Anderson M, Mang H, Plotkin Z, Chan RJ, Dagher PC, p53 is renoprotective after ischemic kidney injury by reducing inflammation. *J. Am. Soc. Nephrol.* 24, 113–124 (2013). [PubMed: 23222126]
39. Ying Y, Kim J, Westphal SN, Long KE, Padanilam BJ, Targeted deletion of p53 in the proximal tubule prevents ischemic renal injury. *J. Am. Soc. Nephrol.* 25, 2707–2716 (2014). [PubMed: 24854277]
40. Megyesi J, Udvarhelyi N, Safirstein RL, Price PM, The p53-independent activation of transcription of p21 WAF1/CIP1/SDI1 after acute renal failure. *Am. J. Physiol.* 271, F1211–F1216 (1996). [PubMed: 8997395]
41. Megyesi J, Safirstein RL, Price PM, Induction of p21WAF1/CIP1/SDI1 in kidney tubule cells affects the course of cisplatin-induced acute renal failure. *J. Clin. Invest.* 101, 777–782 (1998). [PubMed: 9466972]
42. Bates S, Rowan S, Vousden KH, Characterisation of human cyclin G1 and G2: DNA damage inducible genes. Oncogene 13, 1103–1109 (1996). [PubMed: 8806701]
43. Shimizu A, Nishida J.-i., Ueoka Y, Kato K, Hachiya T, Kuriaki Y, Wake N, CyclinG contributes to G2/M arrest of cells in response to DNA damage. *Biochem. Biophys. Res. Commun.* 242, 529–533 (1998). [PubMed: 9464250]
44. Huang S, Susztak K, Epithelial plasticity versus EMT in kidney fibrosis. *Trends Mol. Med.* 22, 4–6 (2016). [PubMed: 26700490]

45. Grande MT, Sánchez-Laorden B, López-Blau C, De Frutos CA, Boutet A, Arévalo M, Rowe RG, Weiss SJ, López-Novoa JM, Nieto MA, Snail1-induced partial epithelial-to-mesenchymal transition drives renal fibrosis in mice and can be targeted to reverse established disease. *Nat. Med.* 21, 989–997 (2015). [PubMed: 26236989]

46. Wen W, Ding J, Sun W, Fu J, Chen Y, Wu K, Ning B, Han T, Huang L, Chen C, Xie D, Li Z, Feng G, Wu M, Xie W, Wang H, Cyclin G1-mediated epithelial-mesenchymal transition via phosphoinositide 3-kinase/Akt signaling facilitates liver cancer progression. Hepatology 55, 1787–1798 (2012). [PubMed: 22271581]

47. Popov Y, Sverdlov DY, Sharma AK, Bhaskar KR, Li S, Freitag TL, Lee J, Dieterich W, Melino G, Schuppan D, Tissue transglutaminase does not affect fibrotic matrix stability or regression of liver fibrosis in mice. Gastroenterology 140, 1642–1652 (2011). [PubMed: 21277850]

48. Cabibi D, Bronte F, Porcasi R, Ingrao S, Giannone AG, Maida M, Bavetta MG, Petta S, Marco VD, Calvaruso V, Comparison of histochemical stainings in evaluation of liver fibrosis and correlation with transient elastography in chronic hepatitis. *Anal. Cell. Pathol.* 2015, 431750 (2015).

49. Qian HS, Weldon SM, Matera D, Lee C, Yang H, Fryer RM, Fogo AB, Reinhart GA, Quantification and comparison of anti-fibrotic therapies by polarized SRM and SHG-based morphometry in rat UUO model. PLOS ONE 11, e0156734 (2016). [PubMed: 27257917]

50. Canaud G, Bienaimé F, Tabarin F, Bataillon G, Seilhean D, Noël L-H, Dragon-Durey M-A, Snanoudj R, Friedlander G, Halbwachs-Mecarelli L, Legendre C, Terzi F, Inhibition of the mTORC pathway in the antiphospholipid syndrome. *N. Engl. J. Med.* 371,303–312 (2014). [PubMed: 25054716]

51. Brooks C, Wei Q, Cho S-G, Dong Z, Regulation of mitochondrial dynamics in acute kidney injury in cell culture and rodent models. *J. Clin. Invest.* 119, 1275–1285 (2009). [PubMed: 19349686]

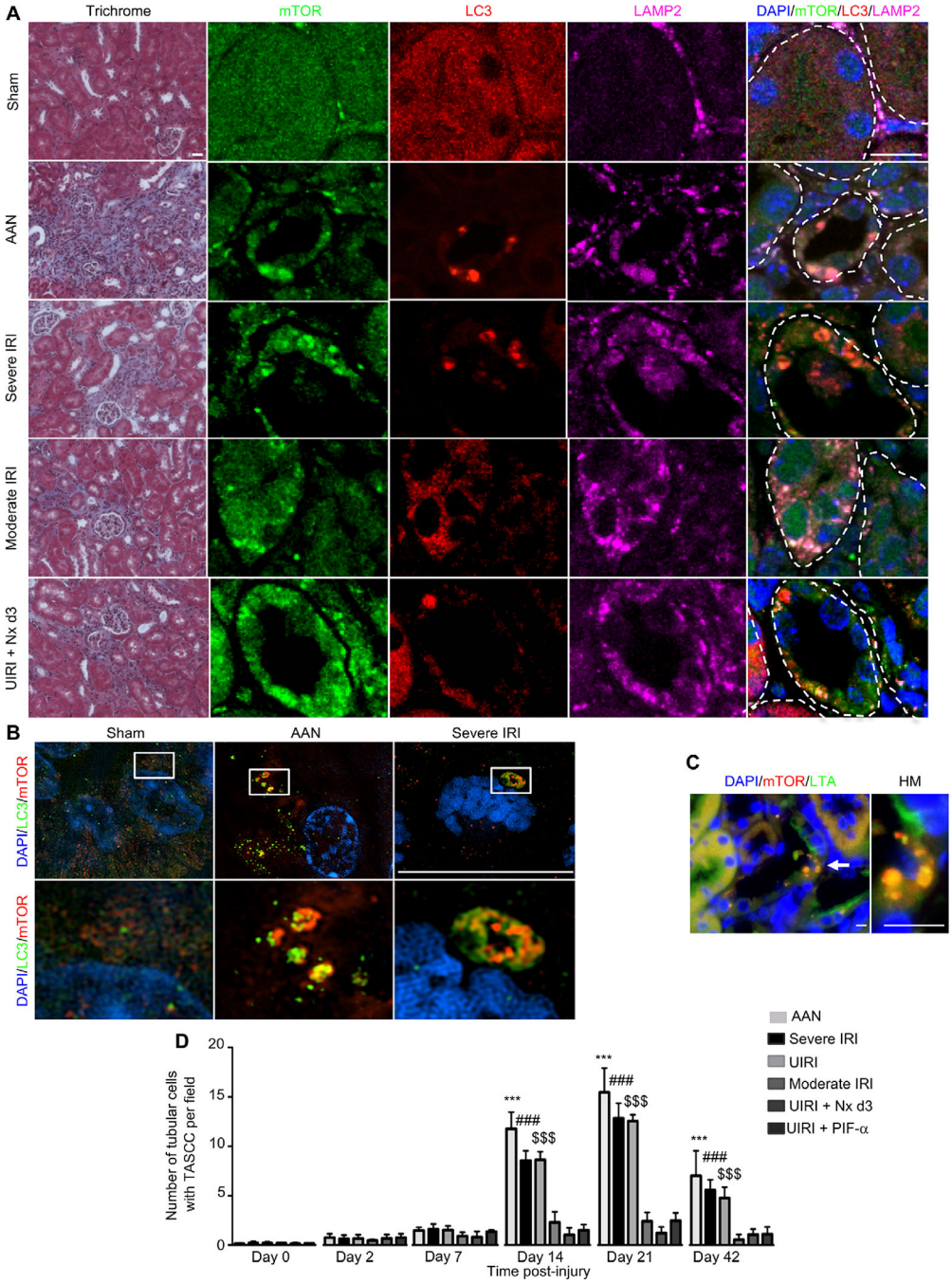

Fig. 1. TASCC formation is seen in kidney tubular cells after injury.

(**A**) Morphology (trichrome) of BALB/c mouse kidneys with colocalization of mTOR, LC3, and LAMP2 in the different models of kidney injury 21 days after initiation of the injury. Tubules are delineated with dotted lines. (**B**) Super-resolution imaging of kidney tissue from sham-operated mice, mice treated with AA, and mice exposed to severe IRI, stained for LC3 and mTOR. Pictures are representative of $n = 6$ mice per group. (**C**) Coimmunostaining for mTOR and LTA in AA-treated mouse kidney tissue. Injured cells with TASCC formation are not stained with LTA due to dedifferentiation but are adjacent to differentiated neighboring

cells positively stained with LTA. (**D**) Quantification of TASCC formation observed in tubular cells per field (×400) in the different models of murine kidney injury ($n = 6$ at each time point). AAN, AA nephropathy; Nx, contralateral nephrectomy; HM, high magnification. Scale bars, 20 μm (trichrome) and 10 μm [immunofluorescence (IF)]. Data are means ± SEM. Mann-Whitney test: $^{***}P < 0.001$, vehicle-treated mice versus AA-injected mice; $^{\#\#\#}P < 0.001$, sham IRI versus severe IRI; $^{\$\$\$}P < 0.001$, sham IRI versus UIRI.

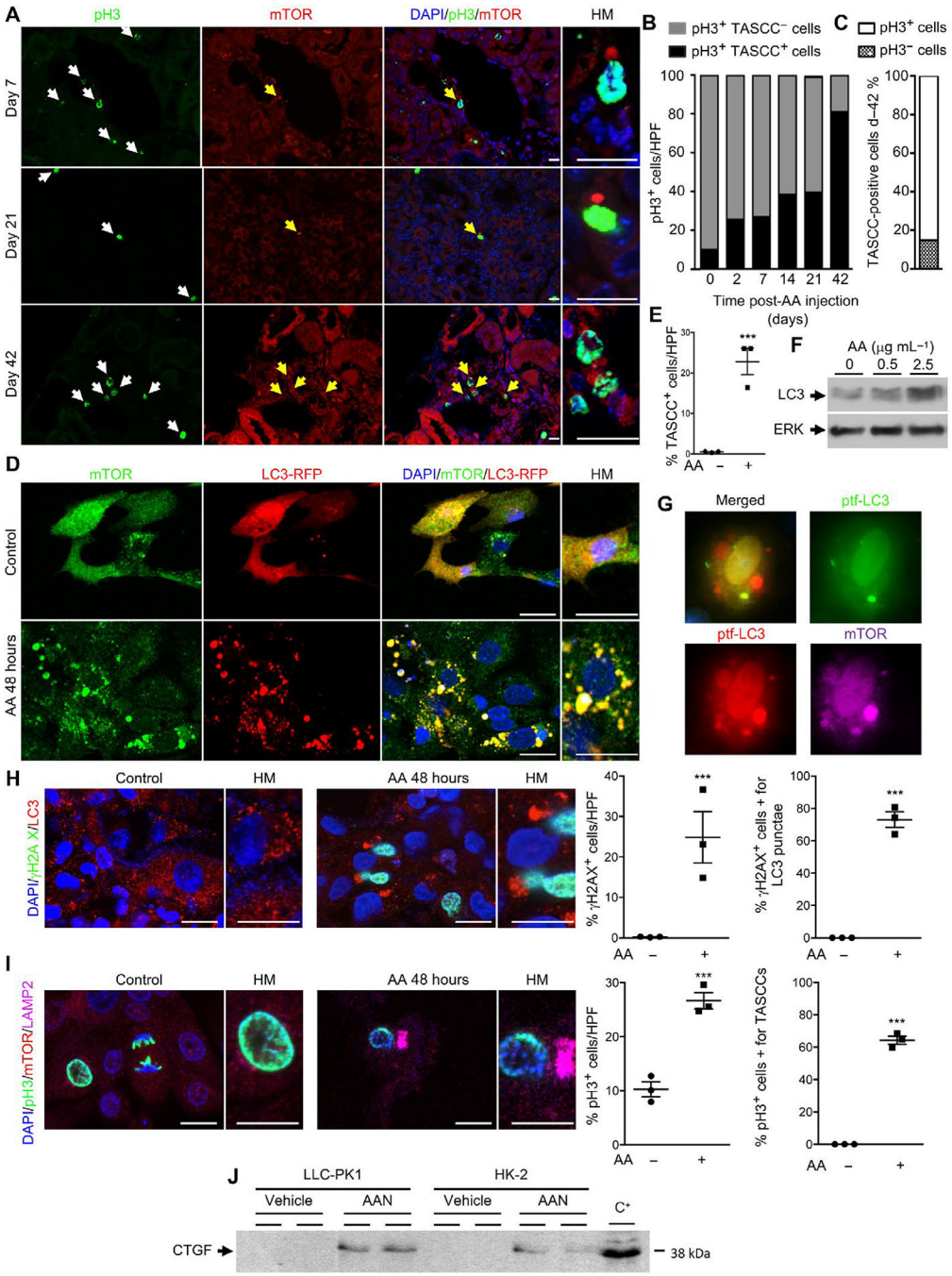

Fig. 2. Kidney proximal tubule cells in the G_2-M phase of the cell cycle are TASCC$^+$.

(A) Coimmunostaining of pH3 and mTOR in mouse kidneys at days 7, 21, and 42 after AA injection (n = 6 at each time point). White arrows, pH3$^+$ nuclei; yellow arrows, TASCC structures. HM, higher magnification. (**B**) Quantification of the percentage of pH3$^+$ cells with TASCC formation per high-powered field (HPF) (×400) after AA injection. (**C**) Percentage of TASCC$^+$ cells per field (×400) coexpressing pH3 42 days after injury. (**D**) Representative mTOR immunostaining in LLC-PK1 cells transfected with LC3-RFP and treated with or without AA (5 μg/ml) for 48 hours. (**E**) Quantification of TASCC$^+$ cells with

mTOR and LC3 staining ($n = 3$ independent experiments). (**F**) Representative Western blot of LC3 accumulation in HK-2 cells treated with or without AA for 48 hours ($n = 3$ independent experiments). (**G**) Representative images of LLC-PK1 cells transfected with ptf-LC3, treated with AA, and stained for mTOR. (**H**) Coimmunostaining and quantification of γH2AX and LC3 in HK-2 cells treated with or without AA (5 μg/ml) for 48 hours. (**I**) Coimmunostaining and quantification of pH 3, mTOR, and LAMP2 in HK-2 cells treated with or without AA (5 μg/ml) for 48 hours. (**J**) Representative Western blot of CTGF in the conditioned medium of HK-2 cells treated with or without AA for 48 hours ($n = 3$ independent experiments). Scale bars, 10 μm. C^+, positive control [conditioned medium from human embryonic kidney (HEK)–293 cells transfected with CG1]. Data are means ± SEM. ***$P < 0.001$ (Student's t test), vehicle administration versus AA administration.

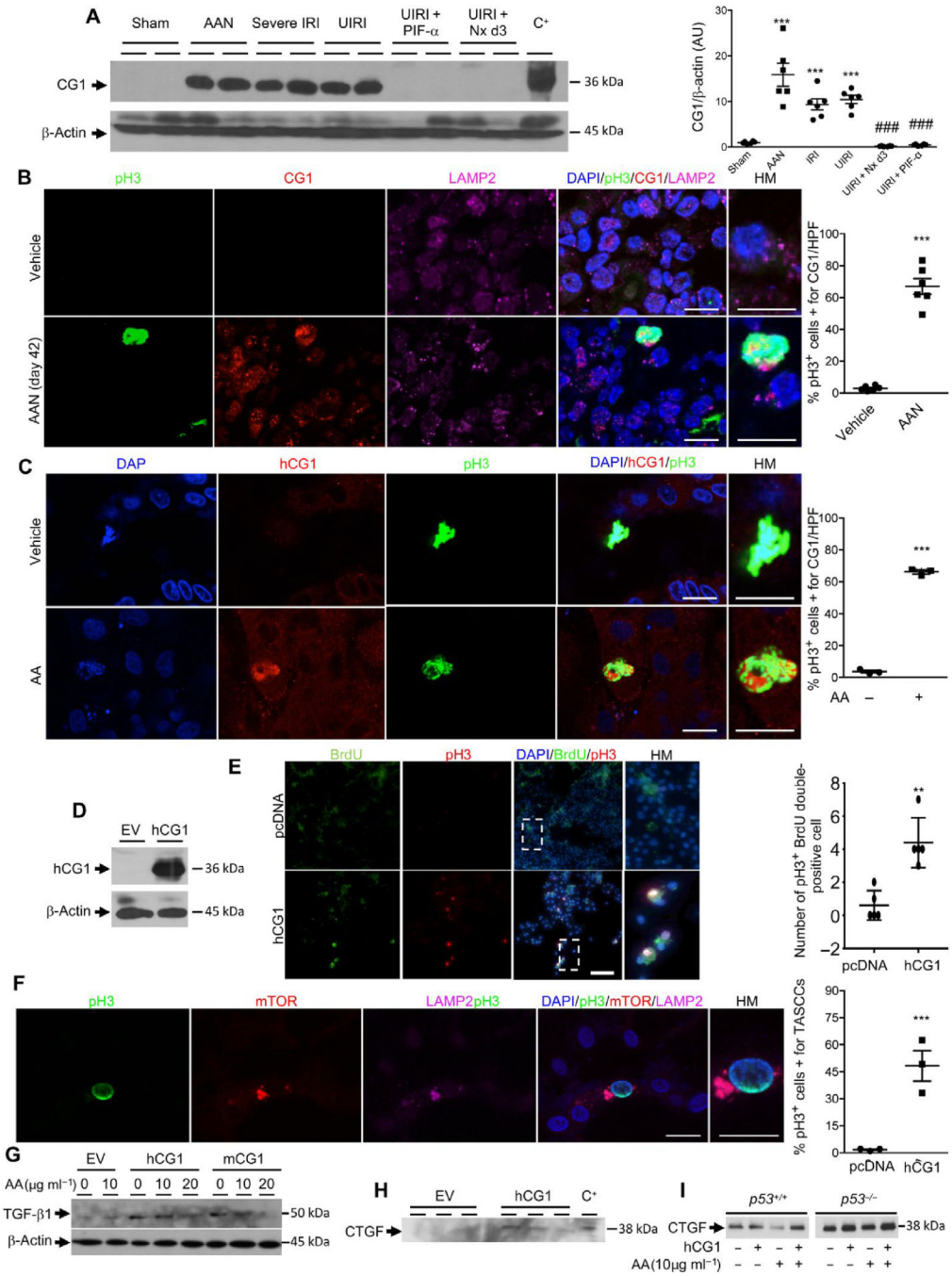

Fig. 3. Kidney proximal tubule cells arrested in G_2-M express CG1.

(**A**) Western blot and quantification of CG1 in mouse kidneys 21 days after various injuries ($n = 6$ animals per group). HEK-293 cells transfected with murine CG1 served as positive control (C^+) for CG1 molecular weight. ***$P < 0.001$ placebo versus AAN, IRI, UIRI. ###$P < 0.001$ UIRI + Nx d3 and UIRI + PIF-A versus AAN, IRI, UIRI. (**B**) Colocalization and quantification of pH3, CG1, and LAMP2 in mouse kidneys 21 days after vehicle or AA injection ($n = 6$ animals per group). ***$P < 0.001$ vehicle versus AAN. (**C**) Colocalization of pH3 and CG1 in HK-2 cells after 48 hours of vehicle or AA treatment. Quantification of

the percentage of cells costained for pH3 and CG1 per high-powered field (×600) ($n = 3$ independent experiments). ***$P < 0.001$ HK-2 vehicle versus HK-2 AA. (**D**) Western blot of CG1 in HK-2 cells transfected with a pCMV empty vector (EV) or the human form of CG1 (hCG1) ($n = 3$ independent experiments). (**E**) HK-2 cells transfected with pCMV EV or vector encoding human CG1 (hCG1), pulse-labeled with BrdU for 3 hours and then fixed 8 hours later. Cells were then stained for BrdU incorporation and pH3. $P = 0.0013$ ($n = 5$). (**F**) Representative images and quantification of coimmunostaining of pH3, mTOR, and LAMP2 in HK-2 cells transfected with hCG1 ($n = 3$ independent experiments). ***$P < 0.001$ pcDNA versus hCG1. (**G**) Western blot of TGF-β1 in HK-2 cells transfected with EV, hCG1, or mCG1 (mouse CG1) after 48 hours of vehicle or AA treatment ($n = 3$ independent experiments). (**H**) Western blot of CTGF secretion into the supernatant of HK-2 cells 48 hours after transfection with either EV- or vector-encoding hCG1 ($n = 3$ independent experiments). HEK-293 cells transfected with the mouse form of hCG1 served as positive control for CTGF molecular weight (C^+). (**I**) HTC-116 p53 wild-type and knockout cells treated with AA with or without transfection with hCG1. Data are means ± SEM. (A) Analysis of variance (ANOVA)-Tukey's post hoc test. (B to I) Student's *t* test. Scale bars, 10 μm (B), (C), and (F); 100 μm (E).

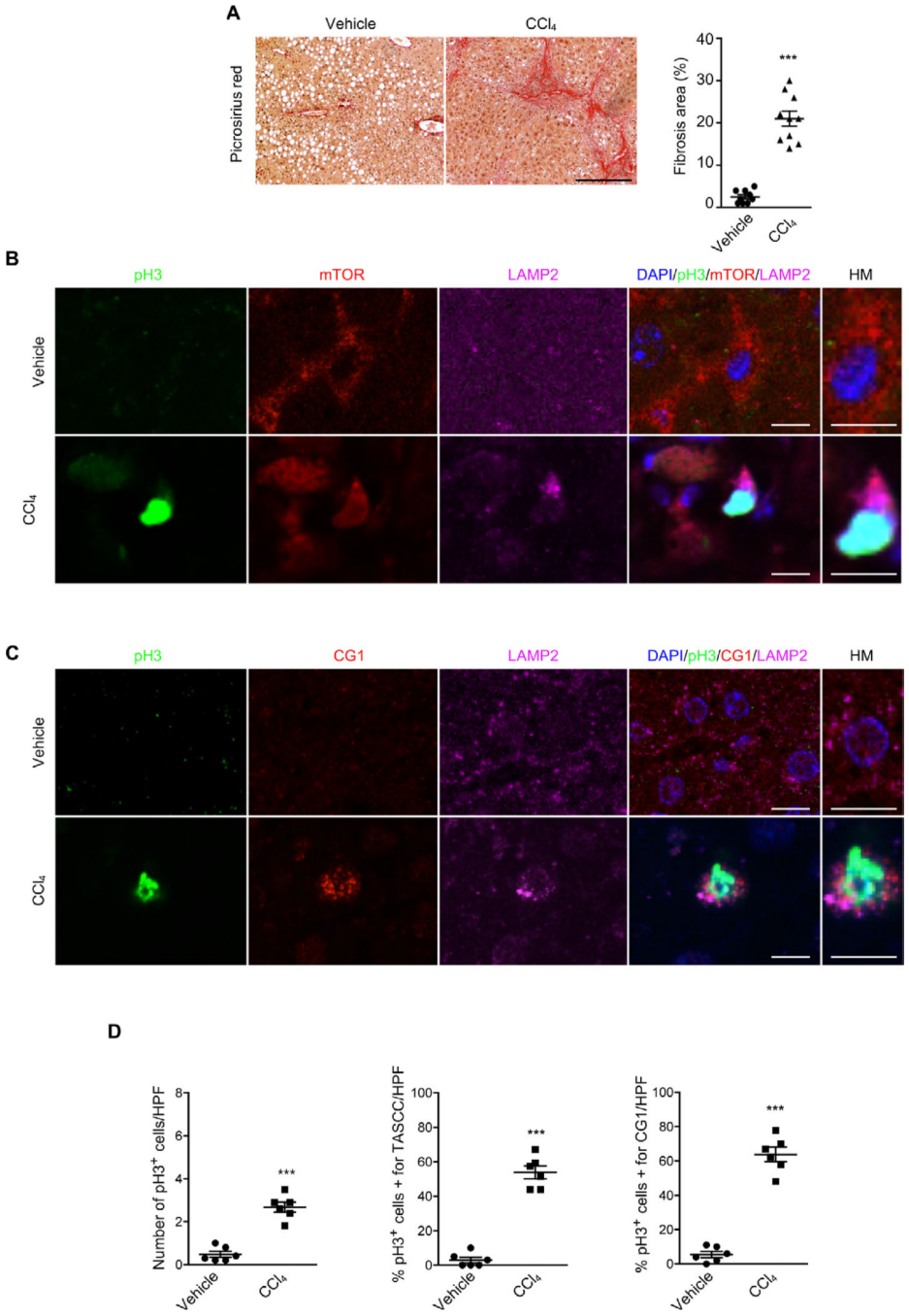

Fig. 4. TASCCs are present in liver G_2-M phase cells during fibrosis progression.

(**A**) Representative picrosirius red images and quantification of liver fibrosis 12 weeks after vehicle or CCl_4 oral gavage (n = 6 mice per group). (**B**) Representative coimmunostaining of pH3, mTOR, and LAMP2 in the liver from mice 12 weeks after vehicle or CCl_4 oral gavage (n = 6 mice per group). (**C**) Coimmunostaining of pH3, CG1, and LAMP2 in the liver from mice 12 weeks after vehicle or CCl_4 oral gavage (n = 6 mice per group). (**D**) Quantification of $pH3^+$, $pH3^+/TASCC^+$, or $pH3^+/CG1^+$ cells per high-powered field (×600). Scale bars, 100

μm (A) and 10 μm (B and C). Data are means ± SEM. ***$P < 0.001$, Student's t test, vehicle versus CCl_4 or CCl_4 oral gavage.

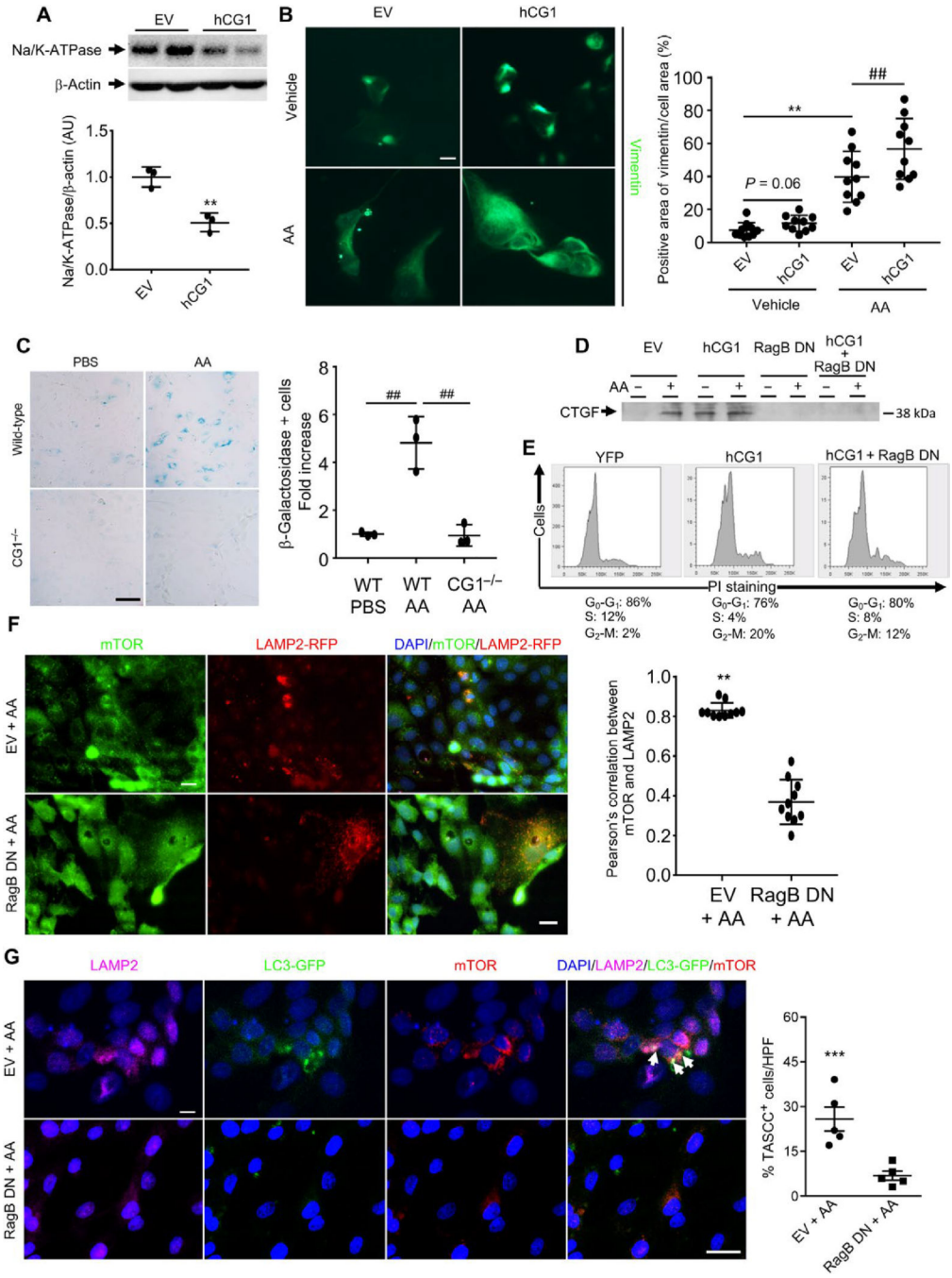

Fig. 5. TASCC disruption reduces the synthesis of fibrotic factors in vitro.

(**A**) Na/K-ATPase expression in LLC-PK1 cells transfected with hCG1 (**$P < 0.01$, EV versus hCG1). (**B**) Immunofluorescence for vimentin in LLC-PK1 cells transfected with hCG1 or EV, treated with AA or vehicle (**$P < 0.01$, $^{\#\#}P = 0.01$). Scale bar, 10 μm. (**C**) β-gal staining of primary proximal tubule cells from wild-type (WT) mice or CG1 knockout mice ($CG1^{-/-}$). Quantification of the fold increase in β-gal-positive cells by cell counting ($n = 3$ independent experiments). Scale bar, 100 μm. $^{\#\#}P < 0.01$. (**D**) Western blot of CTGF in the supernatant of LLC-PK1 cells 48 hours after transfection with EV, human CG1 (hCG1),

dominant negative *RagB* (RagB DN), or both hCG1 + RagB DN and treated with or without AA ($n = 3$ independent experiments). (**E**) Cell cycle analysis by propidium iodide staining and flow cytometry in LLC-PK1 cells 48 hours after transfection with EV, hCG1, or both hCG1 + RagB DN ($n = 3$ independent experiments). (**F**) Immunostaining of mTOR in LLC-PK1 cells transfected with LAMP2-RFP and EV or RagB DN and exposed to AA. Scale bars, 10 μm. $n = 3$ independent experiments. $^{**}P < 0.01$, EV versus RagB DN. The correlation between mTOR and LAMP2 was quantified. (**G**) Coimmunostaining of mTOR, LC3-GFP, and LAMP2 (TASCC, arrowheads) in LLC-PK1 cells transfected with EV or RagB DN and exposed to AA. Scale bars, 20 μm. $n = 3$ independent experiments. $^{***}P < 0.001$, EV + AA versus RagB DN + AA. Data are means ± SEM. (B and C) ANOVA-Tukey's post hoc test. (A and D to G) Student's *t* test.

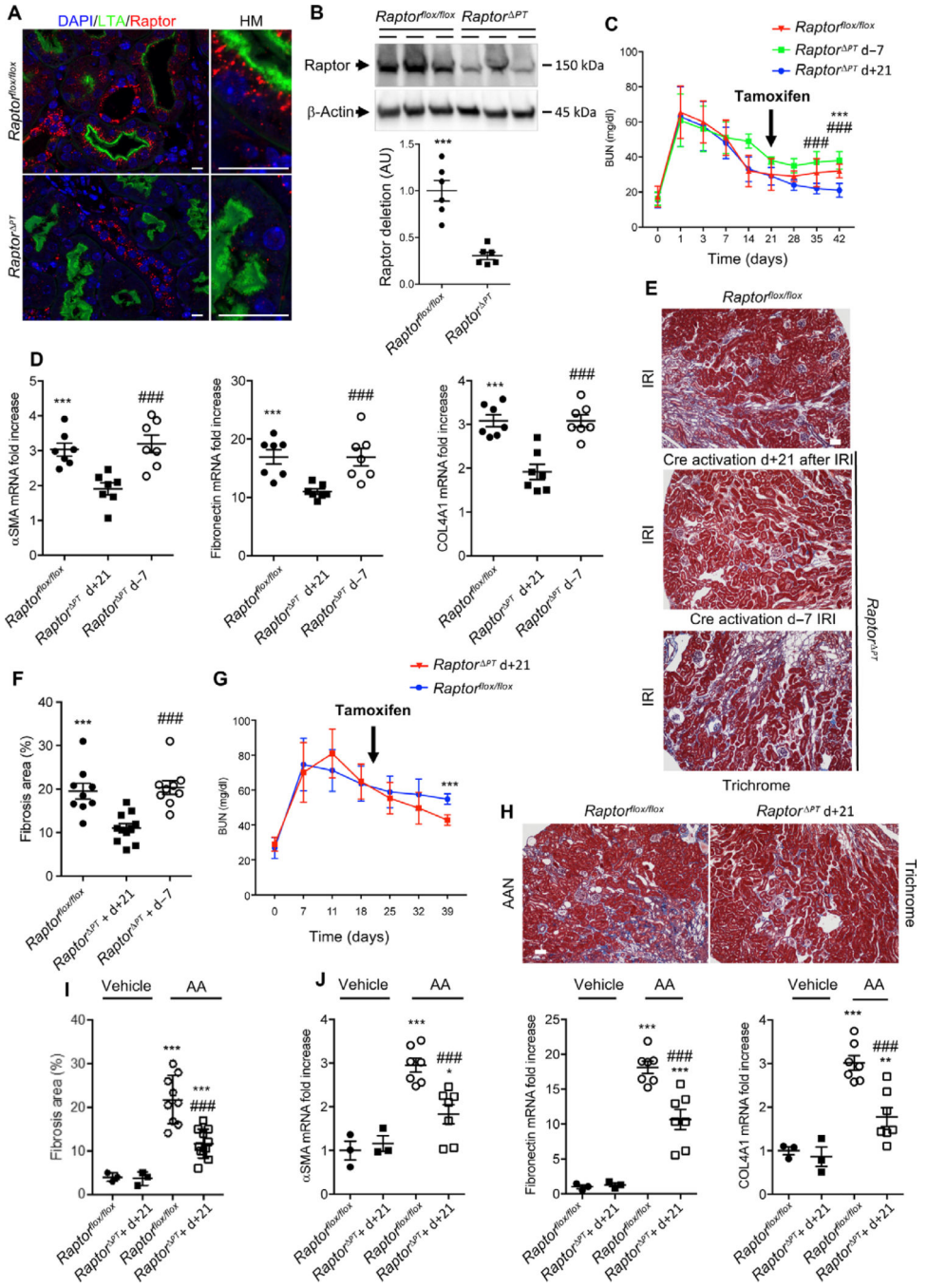

Fig. 6. TASCC disruption reduces profibrotic factor synthesis and kidney fibrosis progression after IRI or AAN.

(A) Coimmunostaining of LTA and Raptor in the *Raptor*$^{flox/flox}$ and *Raptor*$^{\Delta PT}$ mice showing marked Raptor reduction after Cre induction in the LTL^{+} proximal tubule cells. (**B**) Representative Western blot and quantification of Raptor expression from whole-kidney lysates in *Raptor*$^{flox/flox}$ and *Raptor*$^{\Delta PT}$ mice ($n = 12$ per group). $P < 0.001$. (**C**) BUN measurements in *Raptor*$^{flox/flox}$, *Raptor*$^{\Delta PT}$ with Cre recombination 7 days before IRI (*Raptor* d−7), and *Raptor*$^{\Delta PT}$ with Cre recombination 21 days after IRI *(Raptor*$^{\Delta PT}$ d+21).

Arrow indicates the time point in which tamoxifen was administered in this latter group. ###$P < 0.001$, *Raptor*$^{\Delta PT}$ *d−7 versus Raptor*$^{\Delta PT}$ d+21; ***$P < 0.001$, *Raptor*$^{flox/flox}$ versus *Raptor*$^{\Delta PT}$ d+21. (**D**) mRNA expression of αSMA, fibronectin, and collagen 4A1 in kidneys from *Raptor*$^{flox/flox}$, *Raptor*$^{\Delta PT}$ d−7, and *Raptor*$^{\Delta PT}$ d+21. ***$P < 0.001$, *Raptor*$^{flox/flox}$ versus *Raptor*$^{\Delta PT}$ d+21; ###$P < 0.001$, *Raptor*$^{\Delta PT}$ d−7 versus *Raptor*$^{\Delta PT}$ d+21. (**E**) Representative trichrome-stained histological sections of kidneys 42 days after IRI in *Raptor*$^{flox/flox}$, *Raptor*$^{\Delta PT}$ d−7, and *Raptor*$^{\Delta PT}$ d+21 mice. (**F**) Fibrosis quantification kidneys from *Raptor*$^{flox/flox}$, *Raptor*$^{\Delta PT}$ d−7, and *Raptor*$^{\Delta PT}$ d+21 mice ($n = 12$ mice per group). ***$P < 0.001$, *Raptor*$^{\Delta PT}$ versus *Raptor*$^{\Delta PT}$ d+21; ###$P < 0.001$, *Raptor*$^{\Delta PT}$ d−7 versus *Raptor*$^{\Delta PT}$ d+21. (**G**) BUN measurement in *Raptor*$^{flox/flox}$ and *Raptor*$^{\Delta PT}$ d+21 after AAN. Arrow indicates the time point in which tamoxifen was administered. ***$P < 0.001$, *Raptor*$^{flox/flox}$ versus *Raptor*$^{\Delta PT}$ d+21. (**H**) Representative trichrome-stained histological sections of kidneys 40 days after AA in *Raptor*$^{flox/flox}$ and *Raptor*$^{\Delta PT}$ d+21 mice. (I) Fibrosis quantification of kidneys from *Raptor*$^{flox/flox}$ and *Raptor*$^{\Delta PT}$ d+21 mice ($n = 12$ mice per group). ***$P < 0.001$, vehicle versus AA; ###$P < 0.001$, *Raptor*$^{flox/flox}$ versus *Raptor*$^{\Delta PT}$ d+21. (**J**) mRNA expression of αSMA, fibronectin, and collagen 4A1 in *Raptor*$^{flox/flox}$ and *Raptor*$^{\Delta PT}$ d+21 with or without AA exposure. ***$P < 0.001$, vehicle versus AA; ###$P < 0.001$, *Raptor*$^{flox/flox}$ versus *Raptor*$^{\Delta PT}$ d+21. Data are means ± SEM. (C to J) ANOVA–Tukey's post hoc test. (B) Student's *t* test. All scale bars, 10 μm.

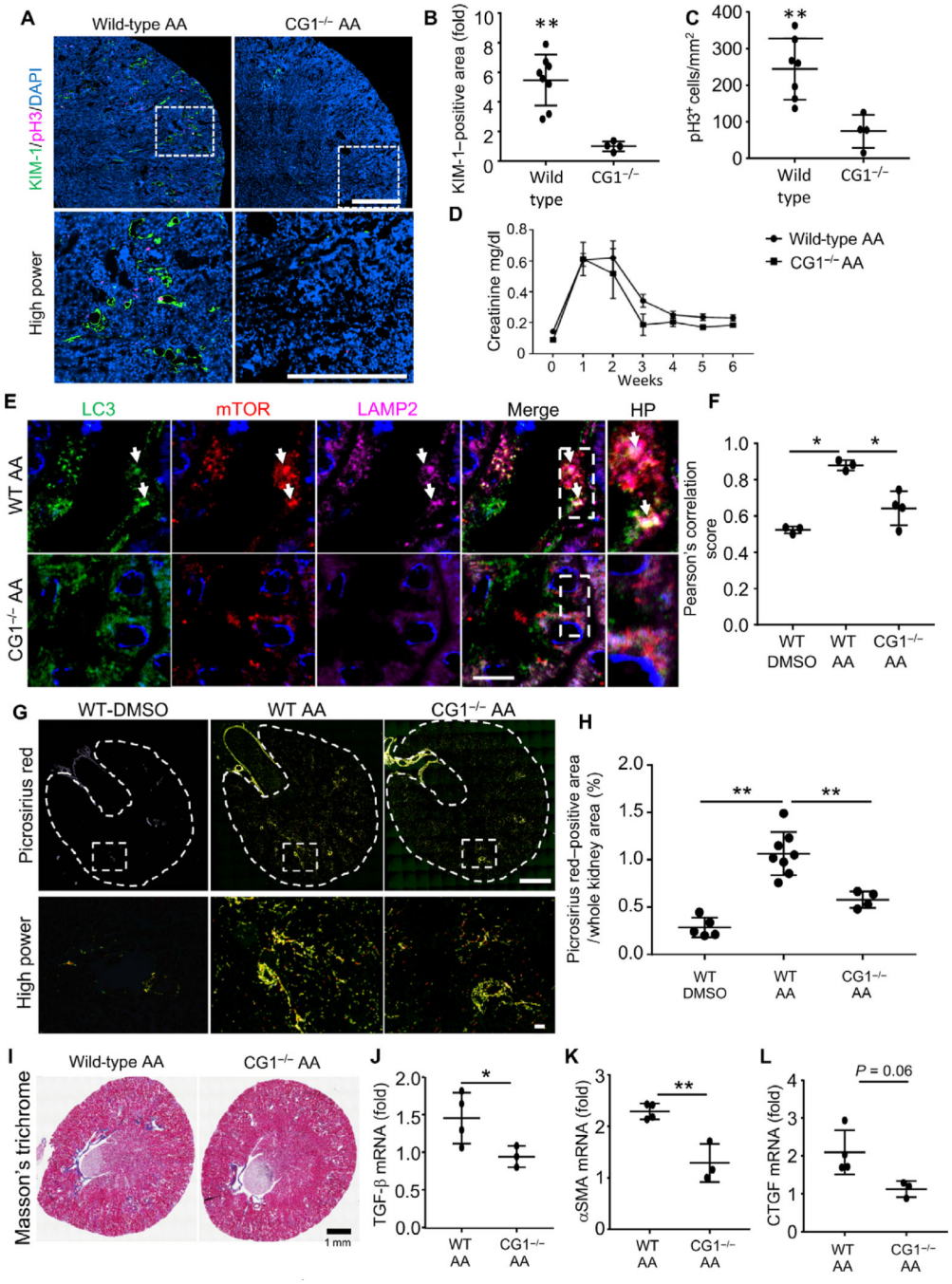

Fig. 7. Deletion of CG1 inhibits TASCC formation and fibrosis.

(**A**) Coimmunostaining of KIM-1 and pH3 in kidneys from wild-type or CG1$^{-/-}$ mice 6 weeks after AA-induced injury. Upper panels: Stitched images representing about 25% of the kidney cross-sectional area taken at ×200 magnification. Lower panels: Higher-magnification images from the boxed regions in the stitched (upper) images. Scale bars, 500 μm. (**B** and **C**) Quantification of KIM-1 and pH3 staining from whole-kidney section images in (A). $n = 4$. (**D**) Serum creatinine from wild-type and CG1$^{-/-}$ mice measured immediately before AA-induced injury and weekly thereafter for 6 weeks. (**E**) Coimmunostaining for

TASCC markers, LC3, mTOR, and LAMP2 in wildtype and $CG1^{-/-}$ kidneys after AA-induced injury. Dashed boxes indicate the high-power (HP) region. Arrows, TASCC structures. Scale bar, 10 μm. (**F**) Quantification of the staining in (E) using NIS Elements software to measure Pearson's colocalization correlation. $n = 3$. (**G**) Upper panel: Imaging of picrosirius red-stained whole-kidney sections from stitched ×100 images using polarized light microscopy. Lower panel: Higher magnification (dashed box) from the stitched images in the upper panel. Dashed line delineates the kidney cortex and medulla regions that were quantified (papillary regions were omitted from quantification). Scale bars, 1 μm (upper) and 100 μm (lower). (**H**) Quantification of the positive area of images in (G). $n = 4$. (**I**) Representative images of Masson's trichrome staining of kidneys from wild-type and $CG1^{-/-}$ mice after AA-induced injury. (**J** to **L**) Quantification of TGF-β, αSMA, and CTGF in wild-type and CG1 kidneys 6 weeks after AA-induced injury by real-time polymerase chain reaction (values are fold change compared to wild-type vehicle-treated mice). $n = 3$. $^{*}P < 0.05$, $^{**}P < 0.01$. Data are means ± SEM. (F and H) ANOVA–Tukey's post hoc test. (A to D and I to L) Student's *t* test. All scale bars, 10 μm.

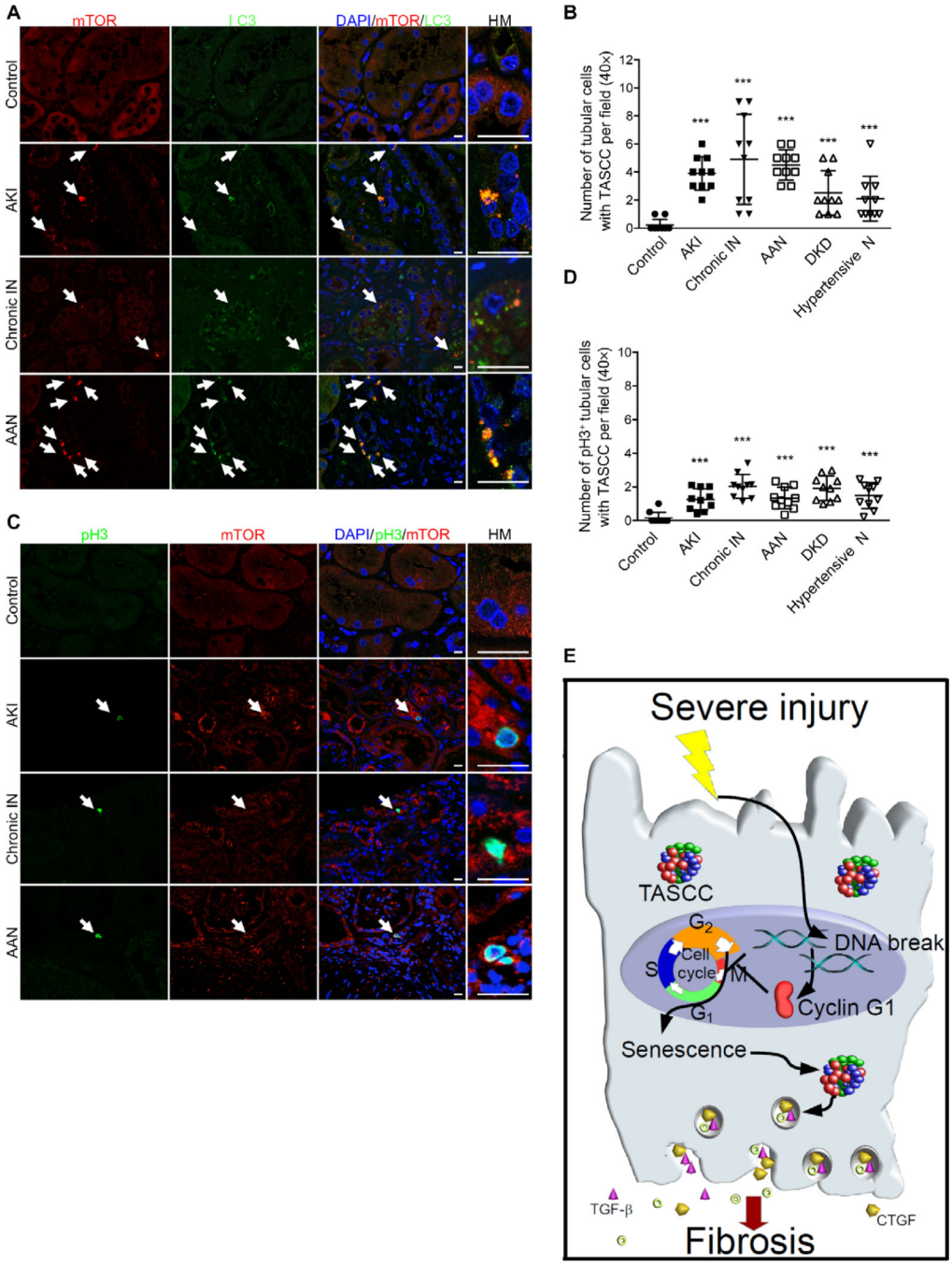

Fig. 8. TASCCs are also observed in human kidney diseases.

(**A**) Coimmunostaining of mTOR and LC3 in biopsies of human control nonfibrotic and fibrotic kidneys [controls (n = 5); AKI (n = 10); chronic interstitial nephritis (Chronic IN) (n = 10); AAN (n = 10); and DKD (n = 10)]. Control tissues are normal-appearing renal peritumoral tissues. Arrows mark TASCCs. (**B**) Quantification of TASCC$^+$ tubular cells per field (×40). (**C**) Colocalization of pH3 and mTOR in human kidney biopsies with fibrosis (n = 10 per group) and controls (n = 5). Scale bars, 10 μm. (**D**) Quantification of pH3$^+$ tubular cells with TASCC per field (40×). Arrows, pH3$^+$ nuclei. Data are means ± SEM. ANOVA–

Tukey's post hoc test. ***$P < 0.001$, controls versus kidney with fibrosis. (**E**) This cartoon summarizes the involvement of CG1, TASCC, cell cycle, and senescence in the development of fibrosis. Severe kidney injury results in substantial DNA damage, leading to activation of CG1 that suppresses G_2-M transition. G_2-M arrest triggers a senescence-like state, initiating the formation of the TASCC organelle, and a TASCC-induced pro-secretory phenotype. Prolonged CG1 expression and the resulting G_2-M arrest and TASCC-induced secretion promotes fibrosis.